MNRAS 000, 1–17 (2022) Preprint 9 December 2022 Compiled using MNRAS LATEX style file v3.0

Discovery of TOI-1260d and the characterisation of the multi-planet system⋆

Kristine W. F. Lam,[1]† J. Cabrera,[1] M. J. Hooton,[2,3] Y. Alibert,[2] A. Bonfanti,[4] M. Beck,[5] A. Deline,[5] H.-G. Florén,[6] A. E. Simon,[2] L. Fossati,[4] C. M. Persson,[7] M. Fridlund,[7,8] S. Salmon,[5] S. Hoyer,[9] H. P. Osborn,[10,11] T .G. Wilson,[12] I. Y. Georgieva,[7] Gr. Nowak,[13,14] R. Luque,[51] J. A. Egger,[2] V. Abidekyan[15,16] R. Alonso,[13,14] G. Anglada Escudé,[17,18] T. Bárczy,[19] D. Barrado,[20] S. C. C. Barros,[15,16] W. Baumjohann,[4] T. Beck,[2] A. Bekkelien,[5] W. Benz,[2] N. Billot,[5] X. Bonfils,[21] A. Brandeker,[6] C. Broeg,[2,10] S. Charnoz,[22] A. Collier Cameron,[12] Sz. Csizmadia,[1] M. B. Davies,[23] M. Deleuil,[9] L. Delrez,[24,25] O. D. S. Demangeon,[15,16] B.-O. Demory,[10] D. Ehrenreich,[5] A. Erikson,[1] A. Fortier,[2] D. Futyan,[5] D. Gandolfi,[26] M. Gillon,[24] M. Guedel,[27] P. Guterman,[9,28] J. Laskar,[29] D. W. Latham, [30] A. Lecavelier des Etangs,[31] M. Lendl,[5] C. Lovis,[4] K. Heng,[10,32] K. G. Isaak,[33] L. Kiss,[34,35,36] D. Magrin,[37] P. F. L. Maxted,[38] V. Nascimbeni,[39] G. Olofsson,[6] R. Ottensamer,[27] I. Pagano,[39] E. Pallé,[13,14] G. Peter,[40] G. Piotto,[37] D. Pollacco,[32] D. Queloz,[41,3] I. Ribas,[17,18] R. Ragazzoni,[37,42] N. Rando,[43] H. Rauer,[1,44,45] N. C. Santos,[15,16] G. Scandariato,[39] S. Seager,[11,46,47] D. Ségransan,[5] L. M. Serrano,[26] A. M. S. Smith,[1] S. G. Sousa,[15] M. Steller,[4] Gy. M. Szabó,[35,48] N. Thomas,[2] S. Udry,[5] V. Van Grootel,[25] N. A. Walton,[49] J. N. Winn.[50]

(Affiliations can be found after the references)

Accepted XXX. Received YYY; in original form ZZZ

ABSTRACT

We report the discovery of a third planet transiting the star TOI-1260, previously known to host two transiting sub-Neptune planets with orbital periods of 3.127 and 7.493 days, respectively. The nature of the third transiting planet with a 16.6-day orbit is supported by ground-based follow-up observations, including time-series photometry, high-angular resolution images, spectroscopy, and archival imagery. Precise photometric monitoring with CHEOPS allows to improve the constraints on the parameters of the system, improving our knowledge on their composition. The improved radii of TOI-1260b, TOI-1260c are $2.36 \pm 0.06 R_\oplus$, $2.82 \pm 0.08 R_\oplus$, respectively while the newly discovered third planet has a radius of $3.09 \pm 0.09 R_\oplus$. The radius uncertainties are in the range of 3%, allowing a precise interpretation of the interior structure of the three planets. Our planet interior composition model suggests that all three planets in the TOI-1260 system contains some fraction of gas. The innermost planet TOI-1260b has most likely lost all of its primordial hydrogen-dominated envelope. Planets c and d were also likely to have experienced significant loss of atmospheric through escape, but to a lesser extent compared to planet b.

Key words: planets and satellites: detection – planets and satellites: individual: TOI-1260b, c, d – stars: individual: TOI-1260 – techniques: photometric – techniques: radial velocities – planets and satellites: composition

1 INTRODUCTION

Precise characterization of the bulk properties of transiting extrasolar planets allows constraining their possible interior composition. This information is used to infer planet formation processes, as it can be used to demonstrate, for example, transport of material in the protoplanetary disk. Additionally, planets orbiting close to their stars suffer from atmospheric erosion processes (see, e.g. Lampón et al. 2021) that further shape their chemical evolution. The CHaracterising ExOPlanet Satellite (CHEOPS) was launched in 2019 to allow the precise characterization of known planetary systems in order to better understand the processes of planetary formation and evolution (Benz et al. 2021). Since the end of commissioning activities in April 2020, CHEOPS has successfully characterised several planetary systems (e.g. Lendl et al. 2020; Hooton et al. 2022), including the discovery of new planets(e.g. Leleu et al. 2021; Delrez et al. 2021), improving our knowledge of planetary sciences.

In this paper we report the discovery of a third planet orbiting the system TOI-1260, which was previously known to host two

⋆ This article uses data from CHEOPS program CH_PR100031.
† E-mail: kristine.lam@dlr.de

planets (Georgieva et al. 2021, Hereafter G21). The nature of the third planet is supported by ground-based follow-up observations, including time-series photometry, high-angular resolution images, spectroscopy, and archival imagery. Precise photometric monitoring with CHEOPS allows to improve the constraints on the parameters of the system, improving our knowledge on their possible composition. In particular, the study of multiplanet systems with sub-Neptune or super-Earths planets is very interesting for planet formation models, as they share the same disk and have evolved in the same timescales, yet with different outcomes (e.g. Kubyshkina et al. 2019b). The study of small planets allows exploring the effect of physical processes resulting in the observed variation of core compositions and envelope sizes (Modirrousta-Galian et al. 2020). Furthermore, multiplanetary systems provide excellent opportunity to study the dependence of planet formation, evolution and habitability on factors such as stellar insolation, age and spectral type (e.g. Weiss et al. 2018a,b; Leleu et al. 2021).

The planetary system around TOI-1260 was first discovered with the Transiting Exoplanet Survey Satellite (TESS; Ricker et al. 2014), a space-borne NASA mission launched in 2018 to survey the sky for transiting exoplanets around nearby and bright stars. It builds on the legacy of the NASA's Kepler space telescope (Borucki et al. 2010) launched in 2009, which was the first exoplanet mission to perform a large statistical survey of transiting exoplanets. One of the goals of the TESS prime mission is to discover 50 exoplanets with radii smaller than $4R_\oplus$ (e.g. Armstrong et al. 2020; Delrez et al. 2021; Lam et al. 2021; and see also the overview of the planet yield during the Prime Mission in Guerrero et al. 2021). Coordinated mass measurements via precise high-resolution spectroscopic follow-up enable accurate inferences about the bulk composition and atmospheric characterization of small exoplanets. To date, there are more than 100 exoplanets smaller than $4R_\oplus$ in the public domain, with many more in the TESS pipeline.

CHEOPS and TESS missions complement each other in their aims, with TESS carrying the weight of the detection efforts, organizing the community for the ground-based support observations, and CHEOPS providing accurate measurements of the planetary radius, allowing detailed characterization of the planetary interiors (e.g. Lacedelli et al. 2022; Wilson et al. 2022).

The paper is structured as follows. Section 2 describes the TESS observations and transit analysis. The CHEOPS observations and its transit analysis is described in Section 3. The HARPS-N data and the spectral analyses are described in Section 4. Section 5 outlines the the model and result of the joint analysis of the TESS, CHEOPS photometry and HARPS-N RVs. Section 6 discusses the results of the global fit, the interior structure of the planets, planet atmospheric evolution model and the possible origin of the planetary system. Finally, the conclusion of our work is presented in Section 7.

2 TESS PHOTOMETRY

TOI-1260 was observed by TESS during sector 14 (between 18 Jul 2019 and 15 Aug 2019 on camera 4, CCD 3) and sector 21 (between 21 Jan 2020 and 18 Feb 2020 on camera 2, CCD 2) in 2-minute short cadence mode. This data set was previously analyzed in G21. The target was further observed in sector 41 (between 23 Jul 2021 and 20 Aug 2021) in 2-minute and 20-second cadence mode. The TESS data were process by the Science Process Operation Centre (SPOC Twicken et al. 2010; Morris et al. 2017). SPOC extracted TESS light curves using a Simple Aperture Photometry (SAP) and known instrumental systematics are corrected in the Presearch Data Conditioning (PDCSAP) light curves (Smith et al. 2012; Stumpe et al. 2012, 2014). The TESS PDCSAP light curves were downloaded from Mikulski Archive for Space Telescopes (MAST[1]) and were used for subsequent analyses.Figure 1 shows the PDCSAP light curves of TOI-1260.

3 CHEOPS PHOTOMETRY

We performed follow-up photometric observations with CHEOPS to refine the radii of the two inner planets and to confirm the presence of the outer planet, scheduling 9 visits between 26 Dec 2020 and 4 Mar 2021.

The discovery paper of TOI-1260b and c (G21) reported a possible third planet, on the basis of a single transit in sector 21, with a number of period aliases in the range 20.3 d < P < 56.3 d. The paper discussed the possibility of the third planet having a period of 16.6 days. At the time, only one clear single transit were observed in the TESS light curves. The 16.6-day signal in the radial velocity (RV) data was not significant due to the period being close to a harmonic of the stellar rotation period. The nature of the 16.6-day signal was uncertain. However, their results encouraged our efforts to confirm the suspected third planet in the system. We used our code to identify possible additional transit signatures in the existing data (the code is described in Osborn et al. 2022). This identified a unique period of 16.6 d, meaning that the transit fell in the gap in sector 14. The available data at that time was used to constrain the possible ephemeris of the putative third planet in the system. The visits that we programmed with CHEOPS lasted between 8.25 and 16.8 hours to cover the transits of planet b and c, as well as to confirm the presence of the third planet candidate. The details of each observation runs are listed in Table 1.

Observations obtained in each visit were processed by the CHEOPS data reduction pipeline (DRP; Hoyer et al. 2020). The pipeline calibrated each image by applying bias, gain, non-linear effects, dark current, and flat field corrections. It also corrects individual calibrated frames from environmental effects such as smearing trails, bad pixels, background, and stray-light pollution. The DRP then performed aperture photometry on the calibrated and corrected images to extract the photometric fluxes. Next, the DRP pipeline provides four sets of light curves by performing aperture photometry on the calibrated images using different aperture sizes ($R_{\rm ap}$). These apertures are RINF ($R_{\rm ap}$ = 22.5"), DEFAULT ($R_{\rm ap}$ = 25"), RSUP ($R_{\rm ap}$ = 30"), and a further aperture OPTIMAL which is optimised for each visit. We used the root-mean-squared (RMS) values of the light curve extracted by different aperture in each visit to assess the the light curves. Apart from the first visit of planet c, the RINF aperture of each visit gives the lowest RMS. Thus the corresponding light curves were use for subsequent analysis. For the first visit of planet c, we used the light curve reduced from the OPTIMAL aperture for subsequent analysis.

It is known that the rotation of the CHEOPS field-of-view along with the orbit of the spacecraft can result in varying background, contaminants, or other non-astronomical sources (e.g. Wilson et al. 2022). This may induce noises in the data and cause short trm trends in the photometric light curve. Fortunately, the DRP pipeline provides basis vectors for CHEOPS which is used to correct and detrend these variabilities in the light curves. For our dataset, we use the open-source Python package `pycheops` (Maxted et al. 2021) to evaluate

[1] https://archive.stsci.edu/tess

the data produced by DRP and found that the light curves showed periodic flux variation that is in phase with the orbit of the spacecraft.

For each visit, we performed simultaneous transit fitting and detrending of a combinations of standard basis vectors used in the decorrelation of CHEOPS data (i.e. background, contamination, smear, x and y centroid positions, and first, second, and third-order harmonics of the roll angle). The Bayesian Information Criterion (BIC) and minimum χ^2 of the model in each visit were assessed separately to select the basis vectors required to optimally detrend each set of light curve. We also used the $add_g lint$ function to remove internal reflection from resulting from the spacecraft rotation cycle in each visit. The detrended CHEOPS light curves were used for our joint model described in Section 5.

4 HOST STAR CHARACTERISATION

TOI-1260 was observed between 14 Jan 2020 and 13 Jun 2020, a campaign in which 33 high resolution spectra (R= 115000) were reported by G21 using the HARPS-N spectrograph (Cosentino et al. 2012). The HARPS-N Data Reduction Software (DRS) pipeline (Cosentino et al. 2014) was used to extract the spectra.

To retrieve the fundamental parameters of TOI-1260, stellar effective temperature, $T_{\rm eff}$, iron abundance relative to hydrogen, [Fe/H], and the surface gravity, $\log g$, we modelled the HARPS-N co-added high resolution spectrum with the spectral analysis package `SME` (Spectroscopy Made Easy; Valenti & Piskunov 1996; Piskunov & Valenti 2017), version 5.22. With atomic and molecular line data from VALD (Ryabchikova et al. 2015), the MARCS 2012 (Gustafsson et al. 2008) atmosphere grids, and a chosen set of fundamental parameters, `SME` calculate synthetic stellar spectra which is fitted to the observations. The models were also checked with the Atlas12 (Kurucz 2013) grids. We followed the modelling procedure explained in (Persson et al. 2018). In summary, we modelled $T_{\rm eff}$ and $\log g$ with the H_α line wings and the Ca I λ=6102 Å, 6122 Å, and 6162 Å triplet, respectively. The model was checked with the Na I doublet at λ=5888 Å and 5895 Å. The abundances and projected stellar rotational velocity, $V \sin i_\star$, were modelled from unblended lines between λ=6000 Å and 6600 Å. The results, listed in Table 2, were checked with the empirical `SpecMatch-Emp` code (Hirano et al. 2018) which were in very good agreement with `SME`. The full set of host star parameters are listed in Table 2.

As recently described in Schanche et al. (2020), we can use a modified version of the infrared flux method (IRFM; Blackwell & Shallis 1977) to determine the stellar angular diameters and effective temperatures of stars through known relationships between these properties, and estimates of the apparent bolometric flux, via a Markov-Chain Monte Carlo (MCMC) approach. We perform synthetic photometry of TOI-1260 by building spectral energy distributions (SEDs) from stellar atmospheric models with the stellar parameters, derived via the spectral analysis detailed above, as priors. To compute the apparent bolometric flux, these fluxes are compared to the observed data taken from the most recent data releases for the following bandpasses; *Gaia* G, G_{BP}, and G_{RP}, 2MASS J, H, and K, and *WISE* W1 and W2 (Skrutskie et al. 2006; Wright et al. 2010; Gaia Collaboration et al. 2021) with the stellar atmospheric models taken from the ATLAS Catalogues (Castelli & Kurucz 2003). We convert the stellar angular diameter to the stellar radius of TOI-1260 using the offset corrected *Gaia* EDR3 parallax (Lindegren et al. 2021) and obtain $R_\star = 0.672 \pm 0.010\, R_\odot$.

Together with $R_\star$, we used the effective temperature and the metallicity to then derive the isochronal mass $M_\star$ and age $t_\star$. Rather than directly adopting [Fe/H] as a proxy for the stellar metallicity, we estimated the α-element abundance by averaging out the [Mg/H] and [Si/H], obtaining $[\alpha/\mathrm{Fe}] = 0.13 \pm 0.13$. Using Eq. (3) from Yi et al. (2001), we finally computed the metallic content of the star ($[\mathrm{M/H}] = 0 \pm 0.15$ dex) from [Fe/H] and [α/Fe]. To make our $M_\star$ and $t_\star$ estimates more robust we employed two different evolutionary models, namely PARSEC[2] v.1.2S (Marigo et al. 2017) and CLES (Code Liègeois d'Évolution Stellaire Scuflaire et al. 2008). In detail, we interpolated the input set ([M/H], $T_{\rm eff}$, and $R_\star$) within pre-computed grids of PARSEC isochrones and tracks through the isochrone placement technique described in Bonfanti et al. (2015, 2016) and we derived a first best-fit pair of mass and age. The code further accounted for $v \sin i$ and $\log R'_{\rm HK}$ as outlined in Bonfanti et al. (2016) to improve the convergence. Instead, the second pair of mass and age was inferred by directly fitting the input set into the evolutionary track built by CLES according to the Levenberg-Marquadt minimisation criterion (Salmon et al. 2021). After carefully checking the consistency of the results outputted by the two codes through the χ^2-test described in Bonfanti et al. (2021a), we finally merged the respective output distributions ending up with $M_\star = 0.679^{+0.095}_{-0.057}\, M_\odot$ and $t_\star = 6.7^{+5.1}_{-5.2}$ Gyr. The host star mass and radius derived in this work are consistent within $\sim$ 1-sigma and we adopt values from this work for subsequent analyses.

5 JOINT LIGHT CURVE AND RADIAL VELOCITY ANALYSIS

A global analysis of the observational data was performed using the `exoplanet` toolkit (Foreman-Mackey et al. 2021). The toolkit implements the probabilistic programming package `PyMC3` (Salvatier et al. 2016) to perform a Bayesian inference using a Hamiltonian Monte Carlo (HMC; Duane et al. 1987) method.

We first removed the out of transit variability in the TESS light curve by first masking the transits in the light curve, then binning the light curve into 1-hour steps. A Gaussian Process (GP) regression model with a simple harmonic oscillator (SHO) kernel, implemented by `celerite2` (Foreman-Mackey et al. 2017; Foreman-Mackey 2018), was then applied to remove the light curve variations.

The joint analysis was subsequently carried out on the "flattened" TESS light curve from the aforementioned best-fit GP photometry model, CHEOPS light curve, and the HARPS-N RV data. The toolkit uses `starry` (Luger et al. 2019) to model the limb darkened transit light curves. To account for the limb darkening parameters of the star, we used the quadratic limb darkening coefficients (u_1, u_2) parameterised by Kipping (2013) in the model for each photometric instrument. Uniform priors were used for the planet orbital periods ($P_{\rm b}$,$P_{\rm c}$ and $P_{\rm d}$), mid-transit times ($T0_{\rm b}$, $T0_{\rm c}$ and $T0_{\rm d}$), planet-to-star radius ratios ($R_{\rm p,b}/R_{\rm star}$, $R_{\rm p,c}/R_{\rm star}$ and $R_{\rm p,d}/R_{\rm star}$) and impact parameters ($b_{\rm b}$, $b_{\rm c}$, $b_{\rm d}$). We account for the instrument zero-point offset between the TESS ($\sigma_{\rm TESS}$) and CHEOPS ($\sigma_{\rm CHEOPS}$) light curves by fitting a mean to the light curves of the two separate instruments. Gaussian priors were used for the stellar mass $M_{\rm star}$ and radius $R_{\rm star}$ based on the results in Section 4. The Keplerian orbits of the three transiting planets are defined by their orbital periods. The planets' respective semi-major axes (a_b, a_c, a_d) can be derived using Kepler's third law and the scaled semi-major axes ($a_{\rm b}/R_{\rm star}$, $a_{\rm c}/R_{\rm star}$, $a_{\rm d}/R_{\rm star}$) were subsequently derived from the fitted stellar radius.

[2] *PA*dova and T*R*ieste *S*tellar *E*volutionary *C*ode: `http://stev.oapd.inaf.it/cgi-bin/cmd`

Table 1. List of CHEOPS observations of TOI-1260. The file key is the unique identifier which corresponds to the dataset used.

File Key	Observation Start	Observation End	Duration [h]	Exposure Time [s]	N_{frames}
CH_PR100031_TG018501_V0200	2020-12-26 23:21	2020-12-27 08:04	8.72	60.0	296
CH_PR100031_TG018502_V0200	2021-01-18 09:34	2021-01-28 18:34	9.00	60.0	270
CH_PR100031_TG018503_V0200	2021-02-02 09:51	2021-02-02 18:15	8.40	60.0	285
CH_PR100031_TG018504_V0200	2021-02-17 10:49	2021-02–17 19:14	8.42	60.0	291
CH_PR100031_TG036501_V0200	2021-01-22 21:31	2021-01-23 04:58	7.45	60.0	273
CH_PR100031_TG036502_V0200	2021-02-01 05:58	2021-02-01 14:13	8.25	60.0	254
CH_PR100031_TG036504_V0200	2021-02-13 18:18	2021-02-14 02:33	8.25	60.0	281
CH_PR100031_TG036505_V0200	2021-02-16 22:17	2021-02-17 06:32	8.25	60.0	280
CH_PR100031_TG038201_V0200	2021-03-04 03:50	2021-03-04 19:10	15.34	60.0	522

Table 2. Stellar parameters of TOI-1260.

Parameter [Unit]	Value.	Note
Identifiers	TIC 355867695	
RA (ICRS Ep. 2016.0)	157.14401106413	1
Dec (ICRS Ep. 2016.0)	+65.85418726790	1
π [mas]	13.6226 ± 0.0147	1
μ_α [mas yr^{-1}]	-177.340 ± 0.012	1
μ_δ [mas yr^{-1}]	-81.693 ± 0.013	1
Effective temperature $T_{\rm eff}$ [K]	4227 ± 85	2
[Fe/H] abundance	−0.1 ± 0.07	2
[Si/H] abundance	−0.02 ± 0.15	2
[Mg/H] abundance	0.09 ± 0.15	2
[α/Fe] abundance	0.13 ± 0.13	2
[M/H] abundance	0 ± 0.15	2
log g [cgs]	4.57 ± 0.05	2
Stellar rotation velocity $v \sin i$ [km s^{-1}]	1.5 ± 0.7	2
Stellar rotation period $P_{\rm rot}$ [d]	30.63 ± 3.81	2
Chromospheric activity log $R'_{\rm HK}$	−4.86	3
Stellar mass $M_{\rm star}$ [$M_\odot$]	$0.679^{+0.095}_{-0.057}$	2
Stellar radius $R_{\rm star}$ [$R_\odot$]	0.672 ± 0.010	2
Stellar density $\rho_{\rm star}$ [g cm^{-3}]	3.43 ± 0.08	2
Bolometric luminosity [$L_\odot$]	0.129 ± 0.004	2
Stellar age [Gyr]	$6.7^{+5.1}_{-5.2}$	2

[1] Gaia Collaboration et al. (2021), [2] this work, [3] Suárez Mascareño et al. (2015)

The TOI-1260 star is moderately active where activity-induced variations were reported by G21. The activity-induced variations in the RVs were modeled by a GP model alongside the three-planet Keplerian model. We chose a `RotationTerm` GP kernel (Foreman-Mackey 2018), which consists of a mixture of two SHO terms to describe the stellar rotation. A uniform prior was used for the log rotation period ($\log P_{\rm rot}$) parameter and the radial velocity semi-amplitudes ($K_{\rm b}$, $K_{\rm c}$, $K_{\rm c}$) in the RV dataset. Finally, we included jitter ($\sigma_{\rm HARPS}$) and mean velocity offset or systemic offset ($\gamma_{\rm HARPS}$) parameters for the RV fit. The host star mass and radius were sampled using a Gaussian prior which is based on our results in Section 4. We note that the best-fit stellar rotation period from our GP model is 30.63 ± 3.81 days. This gives a rotation rate of $2\pi R_{\rm star}/P_{\rm rot}$ = 1.1 km s^{-1} which is consistent with our $V \sin i$ value from Section 4.

The fitted parameters were first optimised with the `scipy.optimize.minimize` function, integrated in the `exoplanet` package, to find the respective maximum a posteriori parameters. These estimates were used to initialise parameters in the sampling space via a "No U-Turn Sampling" (NUTS; Hoffman & Gelman 2011), a gradient-based HMC sampler implemented in `PyMC3`. We initiated 4 sampling chains where each chain has 2000 tuning steps and 2000 draw iterations. The Gelman-Rubin statistic (Gelman & Rubin 1992) of the sample is ≤ 1.003, indicating the chains are converged.

The phase-folded TESS and CHEOPS transit light curves and the corresponding best-fit transit models are shown in Figure 2. The HARPS-N RVs and best-fit three planet RV model is shown in Figure 3. The phase-folded RVs for each planet and their respective best-fit models are shown in Figure 4.

We studied the case where planet eccentricities are allowed to float in the model and found that there are no difference between the zero and non-zero eccentricities models. Hence we adopted the zero eccentricity model. The resulting median parameters and their 1-σ uncertainties are listed in Table 3. The posterior distributions of fitted parameters are shown in the corner plot in Figure A1.

TOI-1260 is a multiplanet system that consists of three transiting exoplanets where the innermost planet TOI-1260b has a radius and mass of 2.41 ± 0.05 $R_\oplus$ and 8.56 ± 1.54 $M_\oplus$, respectively. TOI-1260c has a radius and mass of 2.74 ± 0.07 $R_\oplus$ and 13.20 ± 4.23 $M_\oplus$, respectively, while the outermost planet TOI-1260d has a radius of 3.12 ± 0.08 $R_\oplus$ and a mass of 11.84 ± 7.79 $M_\oplus$, respectively. With the addition of the CHEOPS photometry as well as TESS data

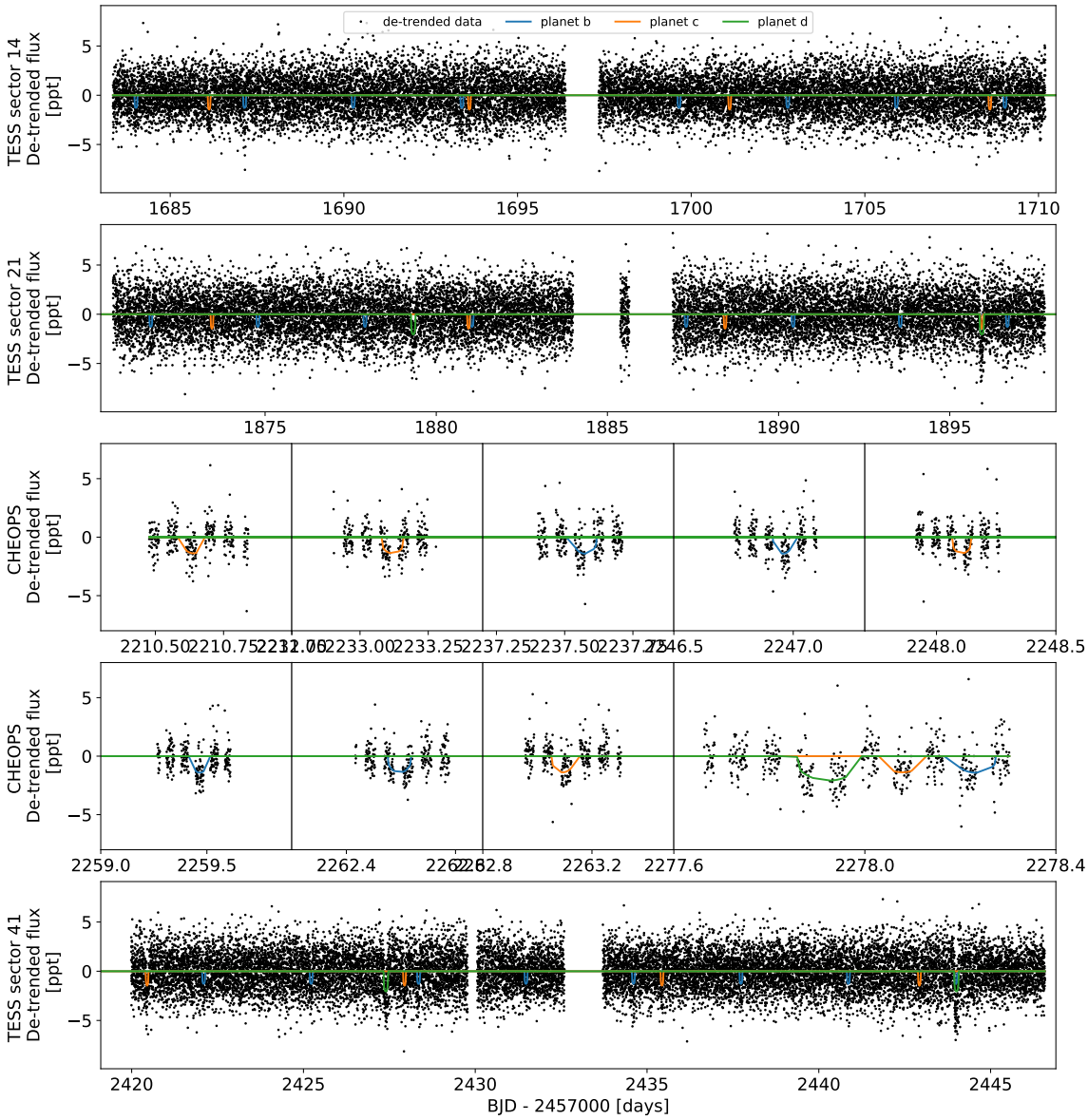

Figure 1. Time-series light curves of TOI-1260. From top to bottom: The TESS PDCSAP light curves from Sectors 14, 21, and 41 are shown in the first, second, and last panels, respectively. The TESS light curves were detrended using a Gaussian Process model described in Section 5. The CHEOPS light curves are shown in the third and fourth rows.

from more recent sectors, this work has significantly improved the precision of the radius measurements of TOI-1260b and c compared to previous work. The radii of all three transiting planets are measured with a precision of better than 3%. We note that the mass precision of planets b and c in our work is does not improve despite the inclusion of planet d in the Keplerian model. This may be due to the methodology used to model the stellar activity induced variation in the RV data. In G21, the author applies a multi-dimensional GP approach and used activity indicators as prior to constraining the GP model which reduced the flexibility of the GP to model the RVs and may have resulted in a smaller semi-amplitude precision. Nevertheless, the